EUROFUSION WPS1-PR(16) 15905

G Dundulis et al.

# Limit analysis of complex welds between plasma vessel and ports in W7-X cryostat system

Preprint of Paper to be submitted for publication in
Fusion Engineering and Design

This work has been carried out within the framework of the EUROfusion Consortium and has received funding from the Euratom research and training programme 2014-2018 under grant agreement No 633053. The views and opinions expressed herein do not necessarily reflect those of the European Commission.

# LIMIT ANALYSIS OF COMPLEX WELDS BETWEEN PLASMA VESSEL AND PORTS IN W7-X CRYOSTAT SYSTEM

G. Dundulis[a], R. Janulionis[a], R. Karalevičius[a], V. Bykov[b], A. Tereshchenko[b] and W7-X team[b]

[a]*Laboratory of Nuclear Installation Safety, Lithuanian Energy Institute, 3 Breslaujos, LT-44403 Kaunas, Lithuania, Gintautas.Dundulis@lei.lt*

[b]*Max-Planck-Institut für Plasmaphysik, Euratom Association, Teilinstitut Greifswald, Wendelsteinstrasse 1, D-17491 Greifswald, Germany*

## Abstract

Fusion is an energy production technology, which could potentially solve problems with growing energy demand in the future. Wendelstein 7-X (W7-X) is an experimental modular stellarator of the HELIAS type, currently in a preparation to the second phase of operation in Greifswald, Germany. The stellarator is a complex 3D structure with high level safety requirements. As a result, sophisticated methods are necessary for the analysis of critical components. The W7-X cryostat mainly consists of the outer vessel, the plasma vessel, and 254 ports with bellows that connect the vessels. The shape of the plasma vessel generally follows the complex shape of the plasma, while ports have different dimensions and are positioned at different inclination angles relative to the vessels. A failure of one port disrupts structural integrity and functionality of the cryostat. Moreover, maintenance and repair are extremely difficult and time-consuming. For this reason, it is very important to evaluate structural strength of the welded connections between the plasma vessel and the ports. The limit analysis by means of finite element method (ABAQUS code) was used to confirm static strength reliability of port welds. According to the results of the analysis it is possible to conclude that the proposed welding between the plasma vessel and the analysed ports fully meets the structural requirements.

**Keywords:** Wendelstein 7-X, Limit load analysis, FEM, Port weld

## 1. Introduction

Wendelstein 7-X (W7-X) is an optimized modular stellarator of the HELIAS type [1, 2] which shall demonstrate the possibility to use such a system for a nuclear fusion power plant in the future. The W7-X is in a preparation to the second phase of operation in Greifswald, Germany by the Max-Planck-Institut für Plasmaphysik (IPP) [3]. A fragment of the W7-X machine is given in Figure 1.

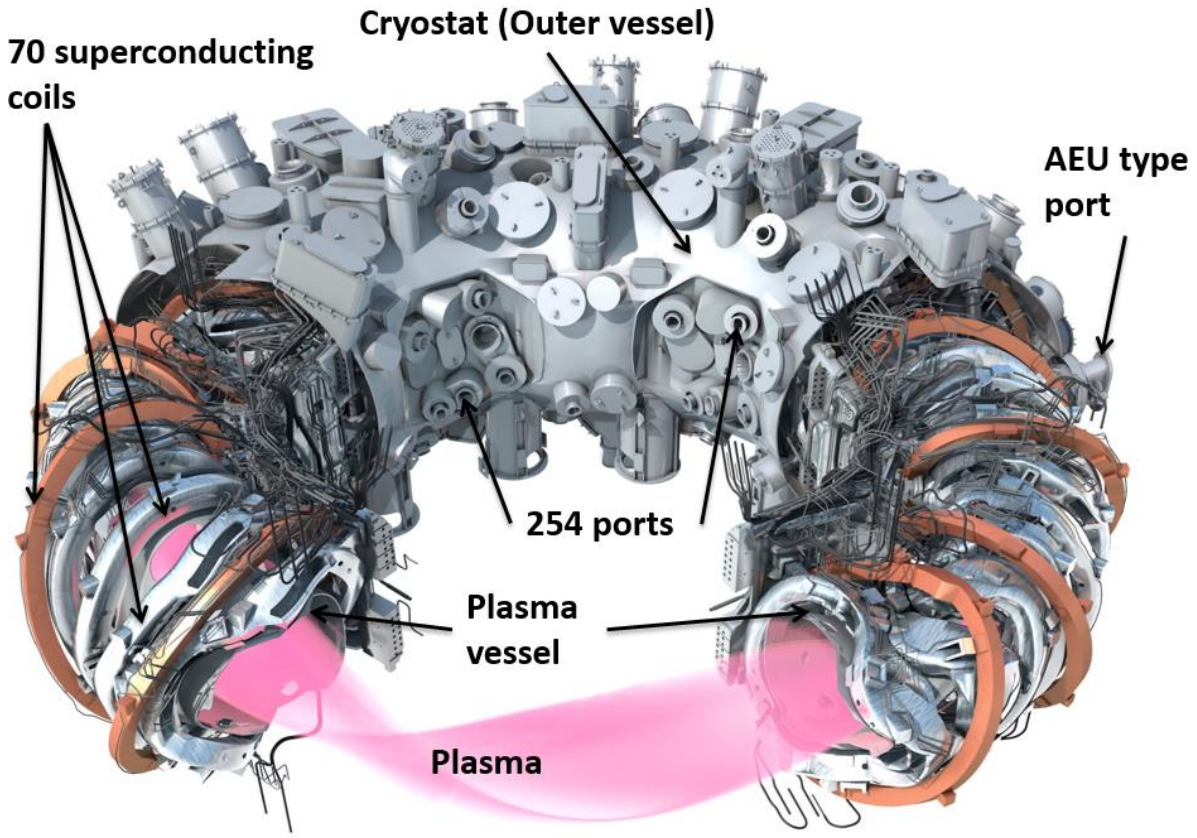


Figure 1. The fragment of a CAD model of the W7-X device

The W7-X cryostat mainly consists of the Outer Vessel (OV), the Plasma Vessel (PV), and 254 ports with bellows that connect the vessels [2, 4]. The PV is the innermost cryostat wall, with its shape generally following the complex shape of the plasma. The PV with in-vessel components provides a physical separation between the plasma and the rest of the stellarator. The PV main body is made from 17 mm thick stainless steel shell covered by thermal insulation on the outer side facing magnet system. The ports have different dimensions, thicknesses (3–15 mm) and inclination angles to the main vessel.

The OV is the vessel that covers the superconducting magnet system. The supply and diagnostic PV ports penetrate the OV/PV interspace between the coils of the magnet system and are attached to the PV at one end and to the OV at the other using bellows to compensate mutual movements of two vessels [4]. The ports provide the only way to access the plasma

and in-vessel components from the outside. Each port is basically a tube with a round, oval, rectangular or with an irregular cross section. In a place where the port is attached to the PV, the PV shell has an opening corresponding to the shape of the port. The port is inserted into the opening in the PV shell until it reaches the inner surface of the shell, and is welded to the PV shell from the inside with a partially penetration weld. During assembly, the other side of the PV shell/port interface is not accessible, because the layout inside the cryostat is designed to minimize the distance between the coils and the thermal insulation of the ports and the vessels. Moreover, minimization of weld throat is necessary to significantly reduce the assembly time and efforts. Due to these facts, the reliable evaluation of the structural integrity of welds is very important for safe operation of the cryostat system.

During operation, the cryostat system of the W7-X stellarator is subjected to many different types of loads applied simultaneously to the same or different parts of the system [2, 5, 6]. The thermal movement of the plasma vessel requires that all ports should be equipped with bellows which vary between 100 mm circular and 1170 mm × 570 mm rectangular sizes. The axial and lateral stiffness of all bellows creates a resulting spring-force which acts directly on the vessel supports [7]. The magnitude of this force varies between different load cases.

On the other hand, the W7-X stellarator has a clear advantage of being a low cycle experimental machine, which is reflected in the choice of codes and standards for the W7-X stellarator, following the same multicode approach as accepted by ITER [8]. Therefore, structural criteria developed for tokamaks such as ITER were correspondingly expanded or relaxed on the basis of tests and experience to achieve a reasonable cost reduction. This approach also includes finite element (FE) limit analyses, which is a powerful method accepted by the project.

Usually limit state criteria are used to design and assess the safety of many engineering components and structures, from simple metal forming problems to large-scale engineering structures and nuclear power plants. Plastic collapse is the limit state of the structure, and the corresponding load is called the limit load. Limit analysis is used to determine the limit load [9–12].

Both analytical and sophisticated numerical methods can be used for calculation of the limit load. One of the most popular analytical methods is the yield-line theory method [13, 14]. The yield-line theory method is employed to achieve fast calculation of the ultimate load. The concept is based on the upper bound of the ultimate load. The yield-line theory method does not require an input of boundary stiffness or an array of structure parameters for modelling non-linearity of the material. The FE method (FEM) is usually used for the limit

load analysis of different structures [15–18]. Numerical methods based on non-linear finite element analyses are increasingly popular, due to complexities of modern devices associated with their geometry and loading conditions. The FE limit analysis is presently performed for estimation of safety criteria (factors) for critical components, welds, handmade insulation, and unique elements [19–21]. Such an analysis can also take into account specific material serration effects observed at low cryogenic temperatures [21].

A reliable prediction of the W7-X structural behaviour is only possible by employing complex FE simulations with a hierarchical set of FE models [22]. The strategy of the W7-X structural analysis [19, 22] is similar to the approaches used for many other unique and large facilities. Two types of models are intensively used: global models for the choice of main system parameters, and local models for detailed analyses of the critical components.

In particular, local models are used for analysis of individual ports. This paper describes a structural integrity analysis of the welded connection in a form of a limit analysis that has been performed for several critical and/or representative port welds. The following welded connections were analysed:

- Welded connection between the port designed for installation of video diagnostic (AEQ20) and the PV shell with a gap between port and shell of 1 mm after port installation (open surface ~ 0.0108 $m^2$);
- Welded connection between the port designed for installation of bolometry and/or tomography and in use for PV horizontal centering system (AEU30) and the PV shell with gaps of 1 mm and 6 mm (open surface ~ 0.0679 $m^2$);
- Welded connection between the port designed for the installation of a complex neutral beam injector (NBI) (AEK20) and the PV shell with a gap of 1 mm (open surface ~ 0.3681 $m^2$).

In this paper, the description of the modelling, methodology of analysis and the analysis results are presented for the big and complex port AEK20 (see Figures 4-b and 5). At end of the paper, in section 4, the summarised results of analysis for the other mentioned ports are also included.

The schematic cross section of the PV and the 12 mm thick AEK20 port weld in the area where the mutual local inclination between shells ($\alpha$) is 90° is presented in Figure 2 for the case with 1 mm gap. The designed curved surface of the weld (the dashed line in Figure 2) was simplified and modelled as such a surface that would project a straight line on the cross section. The FE model of the port has been developed based on the detailed three-dimensional CAD model of the port. The FE limit analyses using elastic-plastic material behaviour has followed the complex geometry modelling. The local FE model of the port was loaded with

forces, moments, and pressure provided by IPP on the basis of the results of the calculations on the global model of the cryostat system.

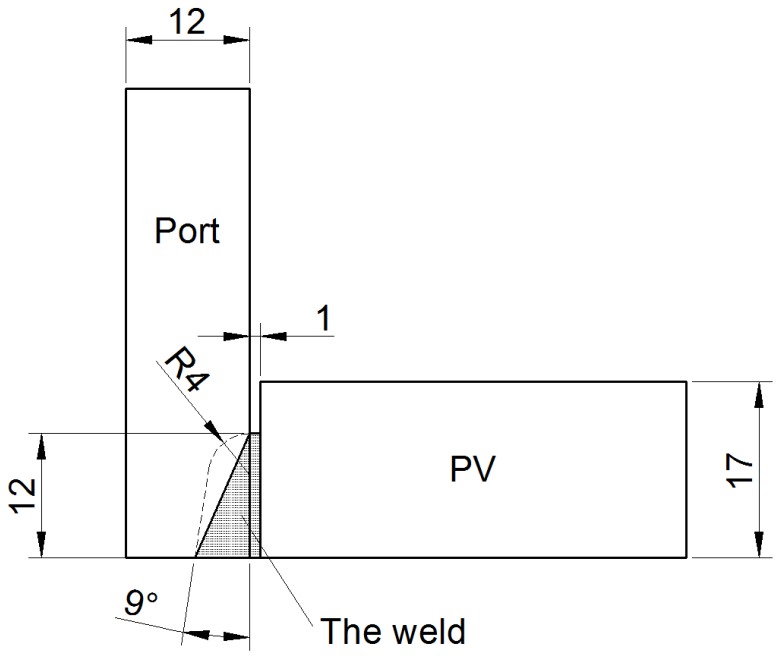


Figure 2. PV/Port weld cross section in the area where the local inclination (α) is 90°

The limit analysis of the AEK20 port welds was performed using the ABAQUS code. The non-linearity of the systems, simplification of the model, other uncertainties and possible variations of nominal parameters were evaluated as presented in the following chapter of the paper.

## 2. FE modelling

The welds between the ports and the PV shell have nonstandard geometry [4, 7, 19, 22]. The port is inserted into the opening in the PV shell in such a way that the end of the port is positioned at the inner surface of the PV shell. Due to geometry of the components there is not enough space to produce a standard type of weld. The distribution of stresses in the weld is very complex and therefore an approach to perform a weld analysis using simple analysis methods or analytical formulas is almost impossible. Moreover, techniques which normally assume that the total stress can be clearly divided into tension, bending and shear components [6] are difficult to use. Due to the fact that the cross section of a closed circular welding seam is much smaller than that of the connected parts, even hoop stresses play, as it turns out, a very significant role here and could not be ignored for the correct weld strength estimation. Therefore, the port selected for this analysis was modelled using the FEM technique as a 3D body together with the regions of the PV shell around the ports and the welding seam. The boundary conditions for the limit analysis of the detailed local FE model of the critical port weld were extracted from the global model of the cryostat [19]. The model was loaded with

corresponding forces, moments, and pressures and subjected to the limit analysis [6]. The limit load analysis was performed by gradually increasing the loads until either the simulation no longer converged, or a very large plastic deformation occurred.

### 2.1 Geometrical and finite element models of the ports welds

The modelling of the welded connection between the port (AEK20) and the PV shell was performed in two steps. First the geometrical 3D models of these port welds were prepared using the SolidWorks software [23]. As the initial geometry of the PV-to-port connection the Lithuanian Energy Institute (LEI) has used a surface model submitted by Max-Planck-Institut für Plasmaphysik (IPP). This surface model consists of a part of the port connected to a small part of the PV as it is modelled in the global model of the cryostat [19]. The detailed refined local FE model developed by LEI includes the central part of main interest modelled by solids and two portions of the PV and the port modelled by shells as in the original model from IPP. The SolidWorks software was used to prepare the solid central part. As the port and the PV have complex shapes, the connection between these parts is even more complex. Therefore, the model of a welded connection could not be developed using simple modelling techniques. It was modelled by creating a big number of sketches around the perimeter of the port-to-PV connection where each sketch represented a cross section of the weld. Later, the sketches were connected using a loft feature (see Figure 3).

The prepared SolidWorks model was transferred to the ABAQUS/Standard FE software [24] to create the finite element model of the welded connection between the port AEK20 and the PV shell. The developed FE model is presented in Figures 4 and 5. The central part includes a portion of the PV, a portion of the port and the full welding seam (see Figures 3-b and -c, Figure 4-b and Figure 5).

### 2.2 Elements used for the models

FE model of the port AEK20 uses linear four node shell elements with reduced integration S4R for the shell part of the port and quadratic eight node shell elements with reduced integration S8R for the shell part of the PV (marked Sh-AEK-1, Sh-AEK-2, and Sh-AEK-3 in Figure 6). The central part, a part of the plasma vessel and a part of the port (marked So-AEK-CP in Figure 6) are modelled as solid bodies and are meshed using 20-node quadratic brick elements with reduced integration C3D20R. The welding seam is meshed using 20-node quadratic brick elements C3D20 [24] (see Figures 4-b and 5). The prepared FE model contains 640284 elements and 2835090 nodes.

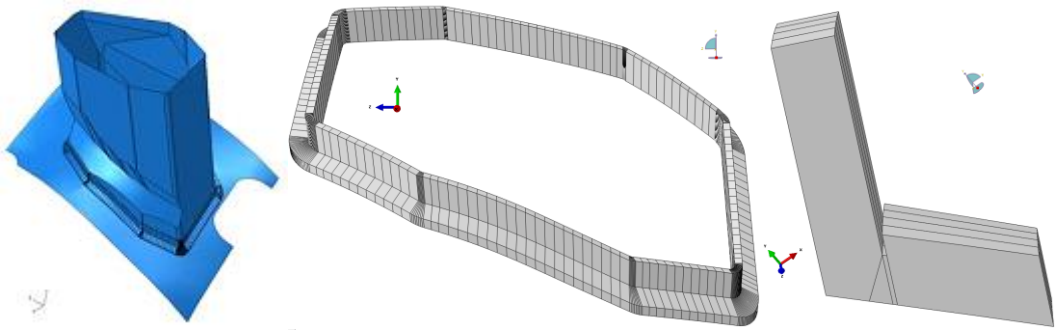

a) b) c)

Figure 3. Geometrical model of the welded connection between the port AEK20 and the PV shell with 1 mm gap: a) model with the weld and parts of the port and the vessel, b) the central part as a solid model (Port, PV, Weld seam), c) the cross section of the central solid part

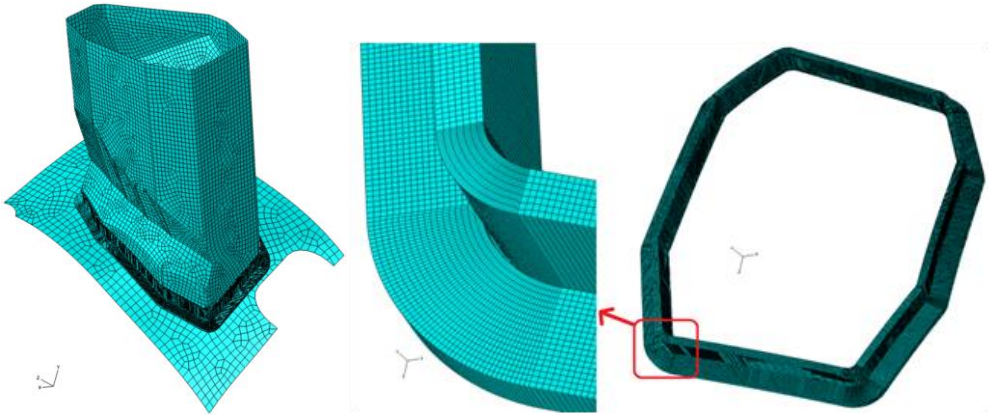

a) b)

Figure 4. FE model of the welded connection between the port AEK20 and the PV shell with 1 mm gap: a) the model of the weld and the parts of the port and the vessel, b) a detail view of the central part meshing

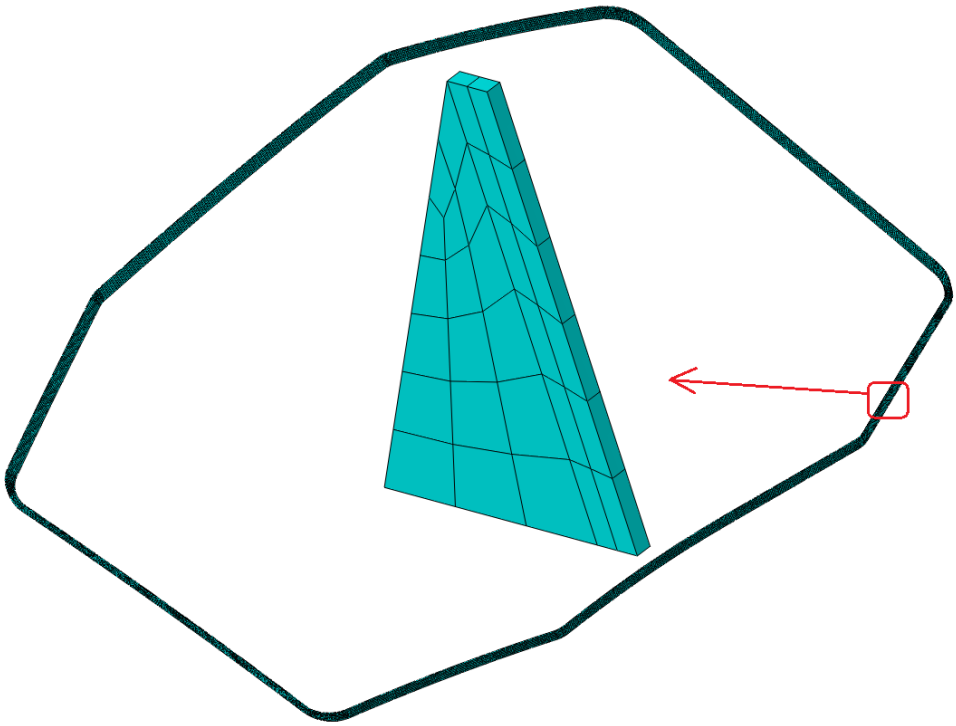

Figure 5. Cross sectional view of the mesh in the welding seam of port AEK20, with 1 mm gap

### 2.3 Geometrical and material data of the port

The geometrical and material data of the welded connection between the port AEK20 and the PV shell are presented in Table 1. The names of the port weld parts used in Table 1 are shown in Figure 6.

Table 1. Material properties [6]

| **Property** | **T, °C** | **Shell-AEK-1** | **Shell-AEK-2** | **Shell-AEK-3** |
|---|---|---|---|---|
| Thickness, mm | – | 16.05 | 14.05 | 4.3 |
| Density, kg/mm$^3$ | 0–100 | $2.0511\times10^{-05}$ | $1.1513\times10^{-5}$ | $1.3214\times10^{-5}$ |
| Young modulus, MPa | 0 | $1.98\times10^{5}$ | | |
| | 20 | $1.96\times10^{5}$ | | |
| | 100 | $1.90\times10^{5}$ | | |
| Poisson's ratio | 0–100 | 0.3 | | |
| Tensile Strength, MPa | 0 | 580 | | |
| | 20 | 580 | | |
| | 150 | 490 | | |
| Yield Strength, MPa | 0 | 320 | | |
| | 20 | 320 | | |
| | 150 | 218 | | |
| Coefficient of thermal expansion, K$^{-1}$ | 0 | $1.60\times10^{-5}$ | | |
| | 20 | $1.61\times10^{-5}$ | | |
| | 100 | $1.67\times10^{-5}$ | | |

## 2.4 Boundary conditions and loads

In order to perform the limit analysis the outer boundaries of the PV were constrained in the following way: the displacements of the edges were fixed in all directions, but the rotations were allowed.

The shell parts of both the port and the PV are connected to the solid FE mesh in the centre (highlighted in magenta) by the shell-to-solid coupling type constrains, showed in Figure 7.

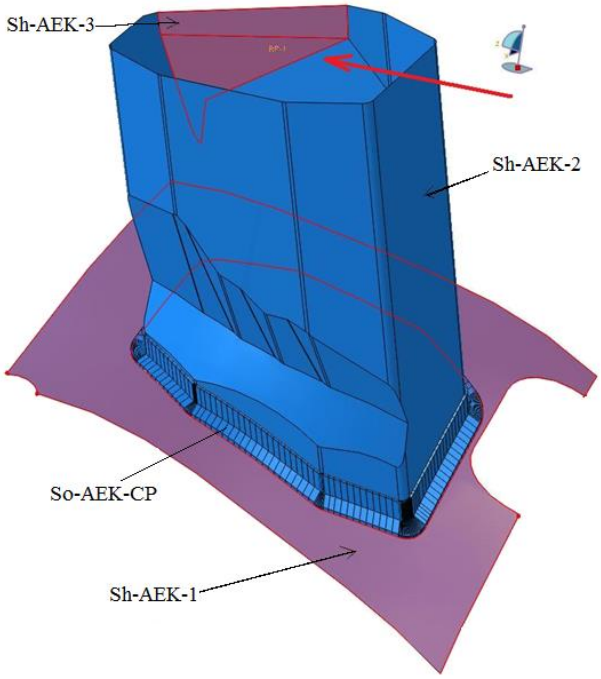


Figure 6. Port AEK20 and the PV shell around it. Red arrow indicates external force application.

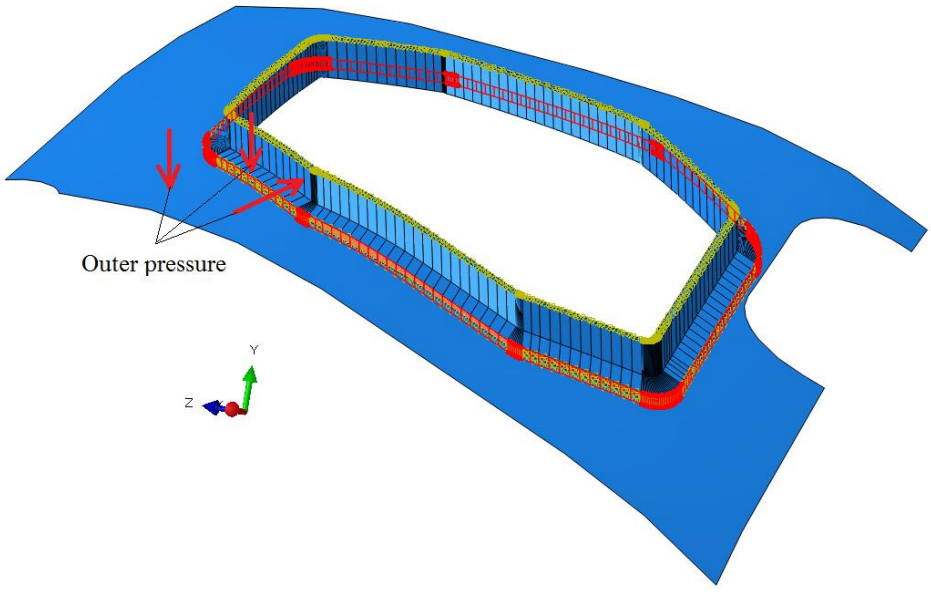


Figure 7. Shell-to-Solid coupling. Red arrows indicate external pressure application.

During operation, the cryostat system of the W7-X stellarator is subjected to many different types of loads applied simultaneously to the same or different parts of the system. Among them there are loads caused by the deadweight of the components and the devices attached to the system on the outside, temperature loads (the PV and the ports are heated to 150° during the baking phase), air pressure loads (up to 1.2 bar in case of abnormal operation), electromagnetic loads, and the loads caused by possible adjustment of the position of the PV. The global models are extensively used for thermal and mechanical analysis, and to extract the boundary conditions in terms of displacements or loads and moments for a separate detailed analysis in critical areas [22]. The approach was also used to load the FE model of the port AEK20 using results of the calculations on the global model of the cryostat system [19]. All load cases are calculated in the assumption that the whole system is linear. The loads listed in Table 2 [6] were applied at the loading step that corresponds to the loading factor of 1.0. The outer pressure was applied to both the solid and shell parts of the PV, the port and the weld as shown in Figure 7. The loads are multiplied by the safety value of 1.2 in order to take possible imprecision of the modelling into account. The safety factor of 1.2 is not applied to gravity.

Table 2. Loads on local FE model

| **Load type** | **Direction** | **Port AEK20** |
|---|---|---|
| Temperature, °C | – | 20 |
| Outer pressure, MPa | – | 0.1013 × 1.2 = **0.1216** |
| **Forces** applied to the end of the port (marked with a thick red arrows in Fig. 8) | $F_x$, kN | -3.706 × 1.2 = **-4.447** |
| | $F_y$, kN | -2.728 × 1.2 = **-3.274** |
| | $F_z$, kN | 2.745 × 1.2 = **3.294** |
| **Moments** applied to the end of the port (marked with a thick red arrows in Fig. 8) | $M_x$, kN×mm | 15039 × 1.2 = **18047** |
| | $M_y$, kN×mm | -13759 × 1.2 = **-16511** |
| | $M_z$, kN×mm | 14640 × 1.2 = **17568** |

Forces and moments were applied to an additional "force-moment" point (FM). The FM point was connected to the port end nodes by the MPC beam type constrain, as showed in Figure 8.

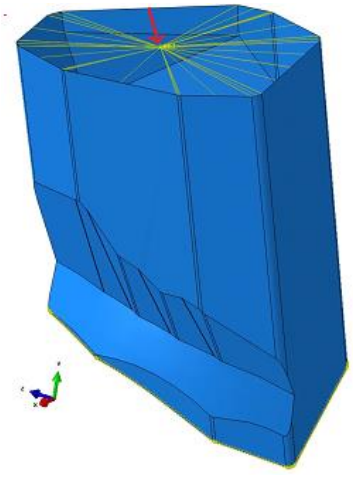

Figure 8. Additional force-moment application point coupled to the port end

The increments which were applied at the loading steps are listed in Table 3. The version 1 (v1) was calculated with the biggest possible stable increment to find out the shape of the displacement-scale factor (SF) dependency curve and to specify the load curve regions where increased increments could be used. Such approach decreases the calculation time. However in regions with pronounced yielding a smaller increment had been chosen to get more reliable results. The version 2 (v2) was calculated with a smaller stable increment to specify the shape of the displacement-SF dependency curve more accurately. The version 3 (v3) employed the adjusted increment calculation strategy: a large increment in case of almost linear dependency and smaller increments in the yielding region, with the smallest increment in the collapse region. It should be noted that the computation efforts strongly depend on the increment size. In the case of the version v3 the calculation took more than two weeks (about 395 hours).

Table 3. Load increment variants for the limit analysis

| $K_{weld}$ | Version | Mesh size | Scale Factor region | Start incr. | Max incr. |
|---|---|---|---|---|---|
| 0.7 | v1 | medium | 0-10 | 0.1 | 1.0 |
| | v2 | medium | 0-10 | 0.05 | 0.075 |
| | v3 | medium | 0-3.5 | 0.15 | 0.4 |
| | | | 3.5-4.5 | 0.15 | 0.45 |
| | | | 4.5-5.5 | 0.03 | 0.06 |
| | | | 5.5-6.1 | 0.02 | 0.006 |

## 3. Results of the limit analysis

Following the approach of limit analysis, the scaling of the loads was performed up to the point where the simulation no longer converges or a very large plastic deformation occurs. Corresponding loads was considered as the critical load. If the main scaling coefficient corresponding to the main critical load was above 1.5, the weld under calculation was considered structurally reliable.

The base material (for the port and the PV shell) was chosen as a material with ideal plasticity at the level of $1.5 \times s_m$. In this analysis the value 320 ($1.5 \times s_m$) MPa for the ideal plasticity yield strength limit was used, where $s_m \cdot = 2/3 \times 320$ MPa. The weld material for all ports was chosen as a material with ideal plasticity at the level of $1.5 \cdot s_m \cdot K_{weld}$. Here $K_{weld}$ is a weld efficiency factor. For this analysis the values $K_{weld} = 0.7$ and $K_{weld} = 0.85$ were used. The analysis was performed at both weld efficiency factor values, but only the analysis results for $K_{weld} = 0.7$ are presented in this article. In the analysis where $K_{weld} = 0.7$, the ideal plasticity value of 224 ($1.5 \times s_m \times 0.7$) MPa was used.

The evolution of the displacement magnitude of the point where loads are applied during limit analysis of the welded connection between the port AEK20 and the PV shell is presented in Figure 9 for version v3 of the analysis.

The results show that displacement of the point, where loads are applied, increases linearly until the scale factor reaches the value of SF = 3.8. The yielding of displacement occurs from SF = 3.8 to SF = 4.5. Over SF = 4.5, the displacement starts to increase very rapidly. The convergence of the FE analysis was lost at SF = 6, and the stability of the port AEK20 with a gap of 1 mm was lost. Therefore, it could be concluded that the limit load is reached at the loading factor of 6.

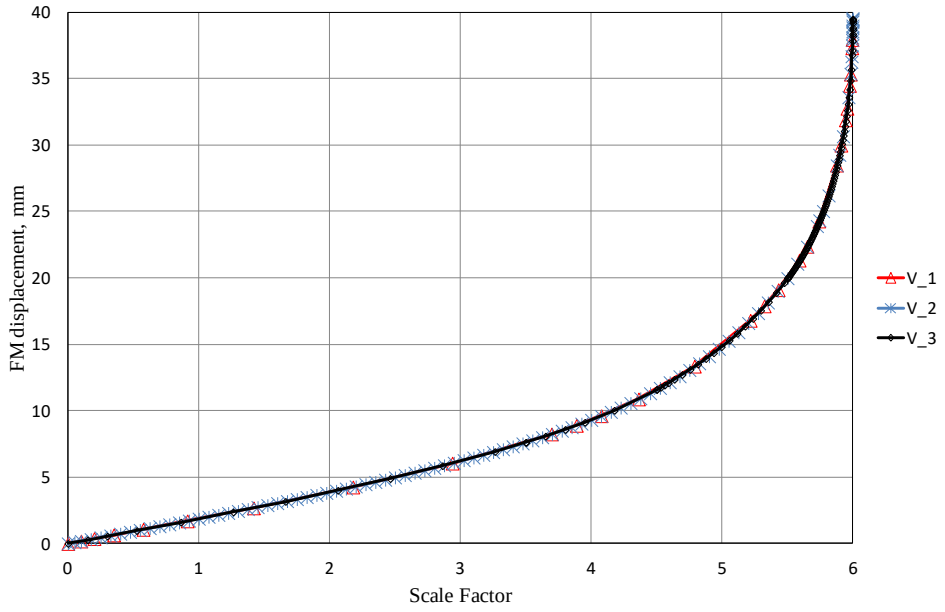


Figure 9. Displacement of force-moment application point. Version v3.

The deformed and undeformed configurations at the end step of the analysis, i.e. at SF = 6, are shown in Figure 10. The maximal displacement magnitude of 41.57 mm is obtained on the wall of the port. The wall of the port is bended due to the applied loads. The bending loading is also transferred to the welding seam of this port.

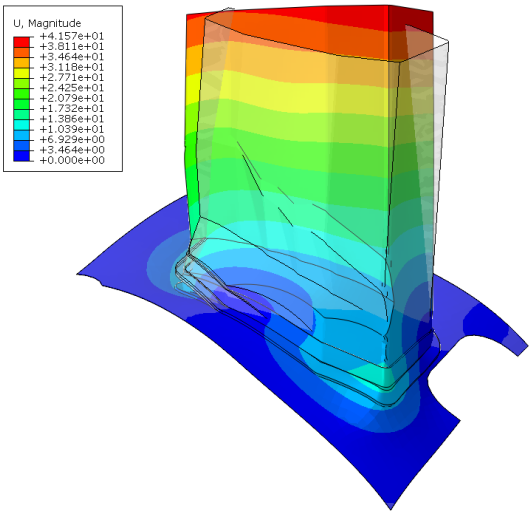


Figure 10. Distribution of displacement in the model AEK20 h1 k07 v3 (displacement scale factor is 15), mm

The maximal obtained artificial stress level is 661 MPa on the weld tip (Figure 11). The stress distribution in the cross section of the weld in the area of the mentioned above maximal stress at the end step of the analysis, i.e., at SF = 6, is presented in Figure 12. The enlarged view of the stress distribution in the weld shows that the stresses reached the values above yield strength in the elements on the top of the weld connected to the PV. The high stress level in the elements on the top of the weld connected to the PV was reached due to a complex shape of the connection. During meshing of the model distorted elements were obtained. Due to the distorted elements, in some areas of the weld, the stress exceeds the ideal plasticity level used in this analysis. The results displayed in Figures 11 and 12 represent the von-Mises stress at the element nodes. When the stress reaches the limit plasticity, the extrapolation of the stress to the element nodes gives higher values while the limit plasticity values (224 MPa) are obtained at element integration points. The von-Mises stress distribution in one element with the highest value is presented in Figure 11, and the actual von-Mises stress values in this element at element nodes and integration points are presented in Fig. 13.

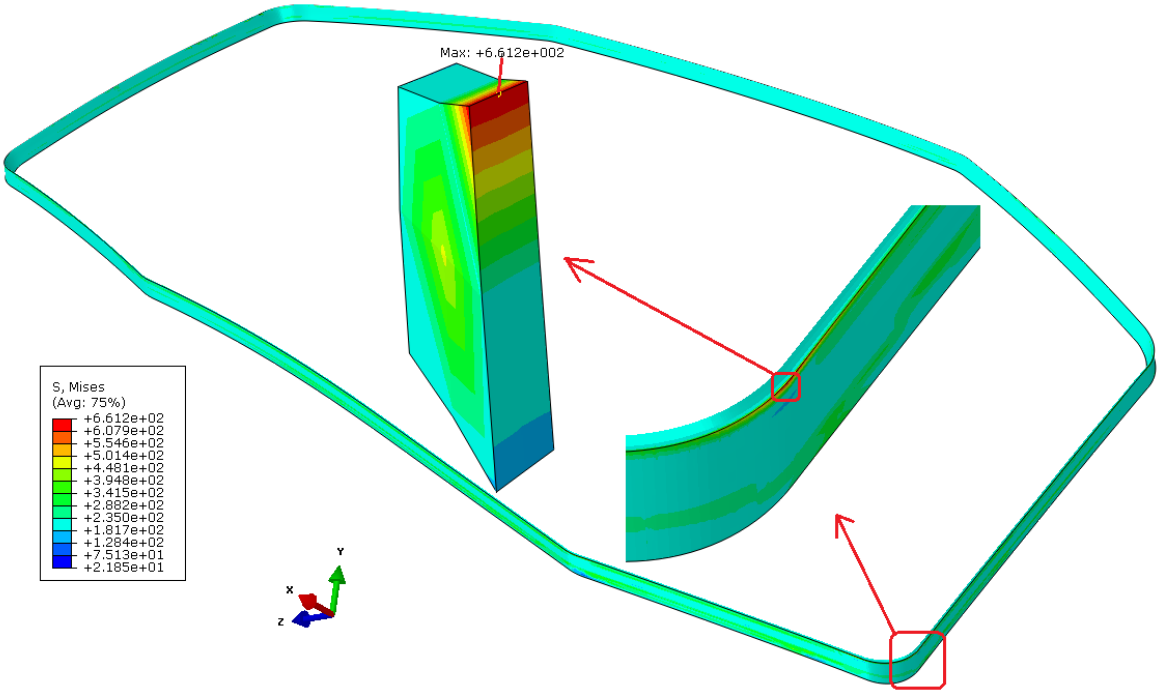


Figure 11. Von Misses Stress distribution (MPa) in the solid-modelled weld, the enlarged view around the maximal stress and an element with the highest artificial stress value of 661 MPa

The distribution of equivalent plastic strain (PEEQ) at the port, the PV and the weld is presented in Figure 14. It was obtained that the whole section of the weld yields at SF=6. The maximal equivalent plastic strain zones are located on the weld tip. According to the stress and equivalent plastic strain results, it is possible to state that failure of the port will have a ductile character.

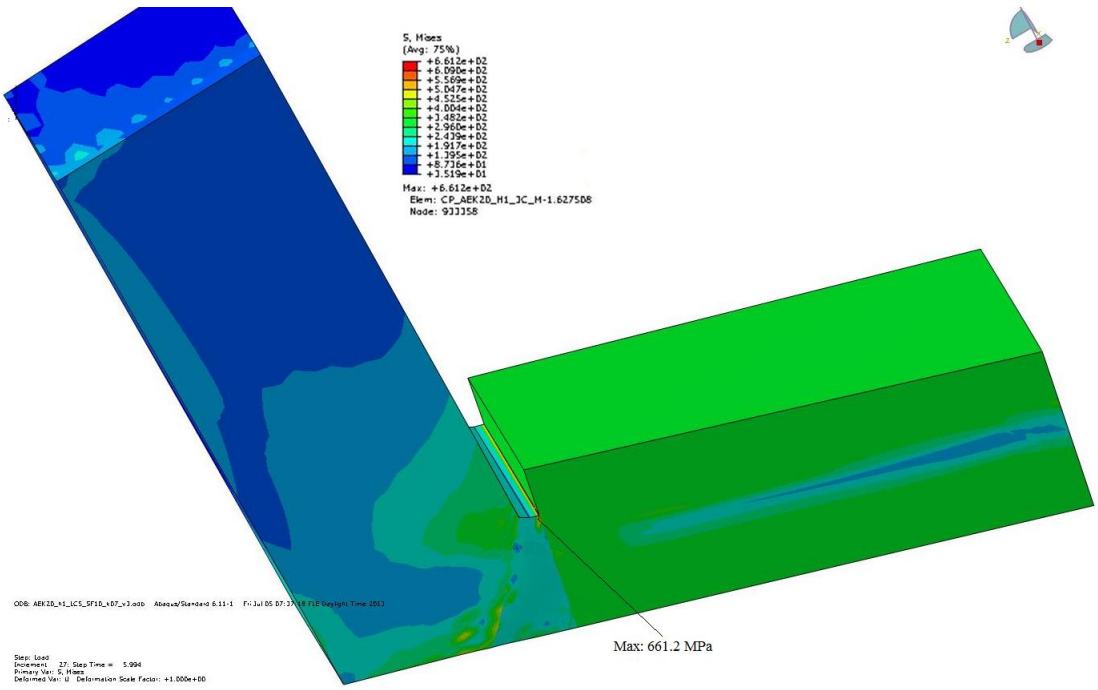

Figure 12. Distribution of von Misses stress (MPa) in the model AEK20 h1 k07 v1, in the cross section of the central part in the area with the maximal stress values

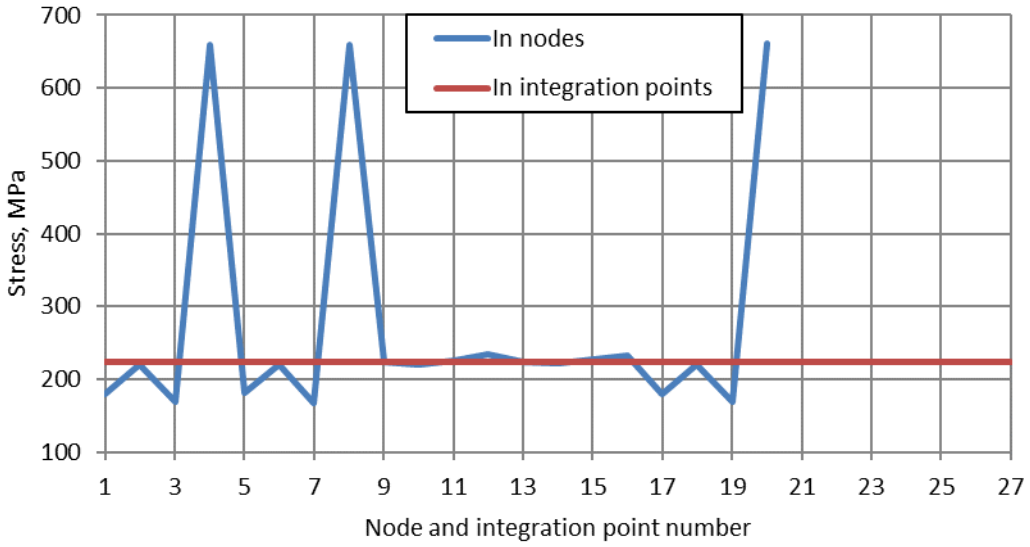


Figure 13. Stress values (MPa) in the element with the highest Von-Mises stress

Stress distribution in the cross section of the weld at the load scaling factor of 3 is presented in Figure 15-a, in the straight part of the weld, and in Figure 15-b, at a point with the maximal artificial stress of 511 MPa (weld corner). As the port has an 8-corner rectangular shape, the higher stress values are reached at the two opposite corners. However, other corners and especially the straight parts of the weld have significantly lower values. As it is shown in Figure 15-b the stress level at the corner reaches the limit plasticity of 224 MPa (at integration points) in the entire cross section of the weld. However, the stress distribution in the cross section of the weld in the straight part of the weld (see Figure 15-a) shows that limit plasticity is reached only at the top corner of the weld, at the point of connection to the PV. The explanation of the high level of stress was already given above.

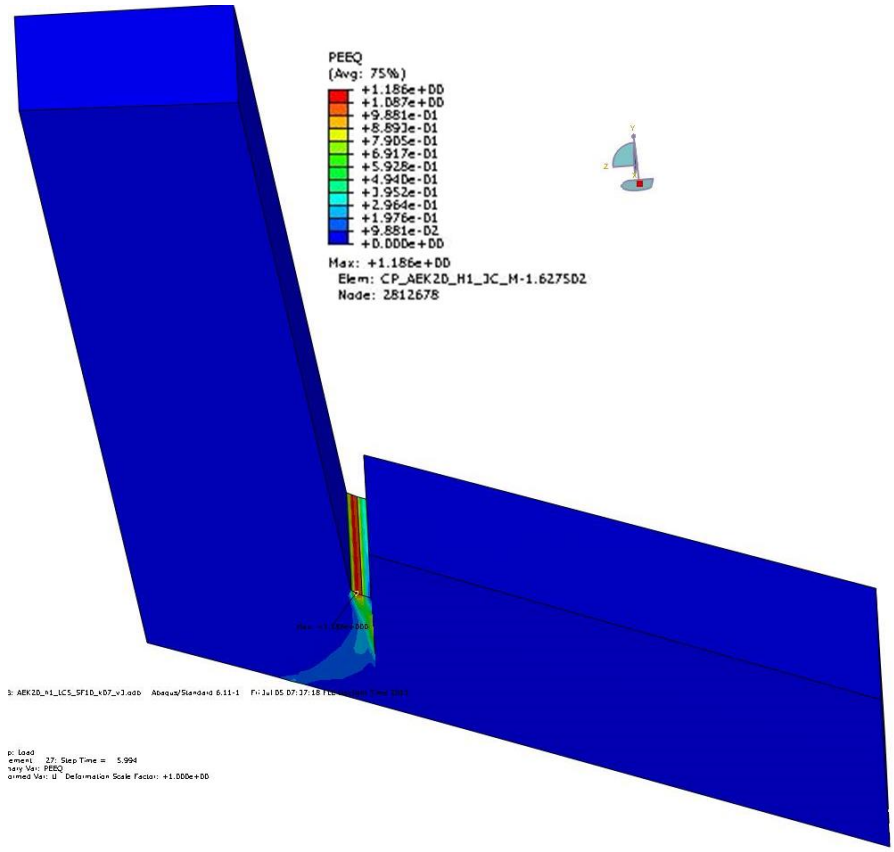


Figure 14. Distribution of equivalent plastic strain in the cross section of the central part of the AEK20 port weld with the maximal stress value

The von Misses stress distribution along the middle line (marked "ML" in Figure 15) of the welding seam and the PV (the perimeter of the weld) is presented in Figure 16. These results confirm that stresses in the weld reach the limit plasticity at two corner parts of the weld that is 5.7% of the length of the perimeter. The mean value of the stress is 135 MPa.

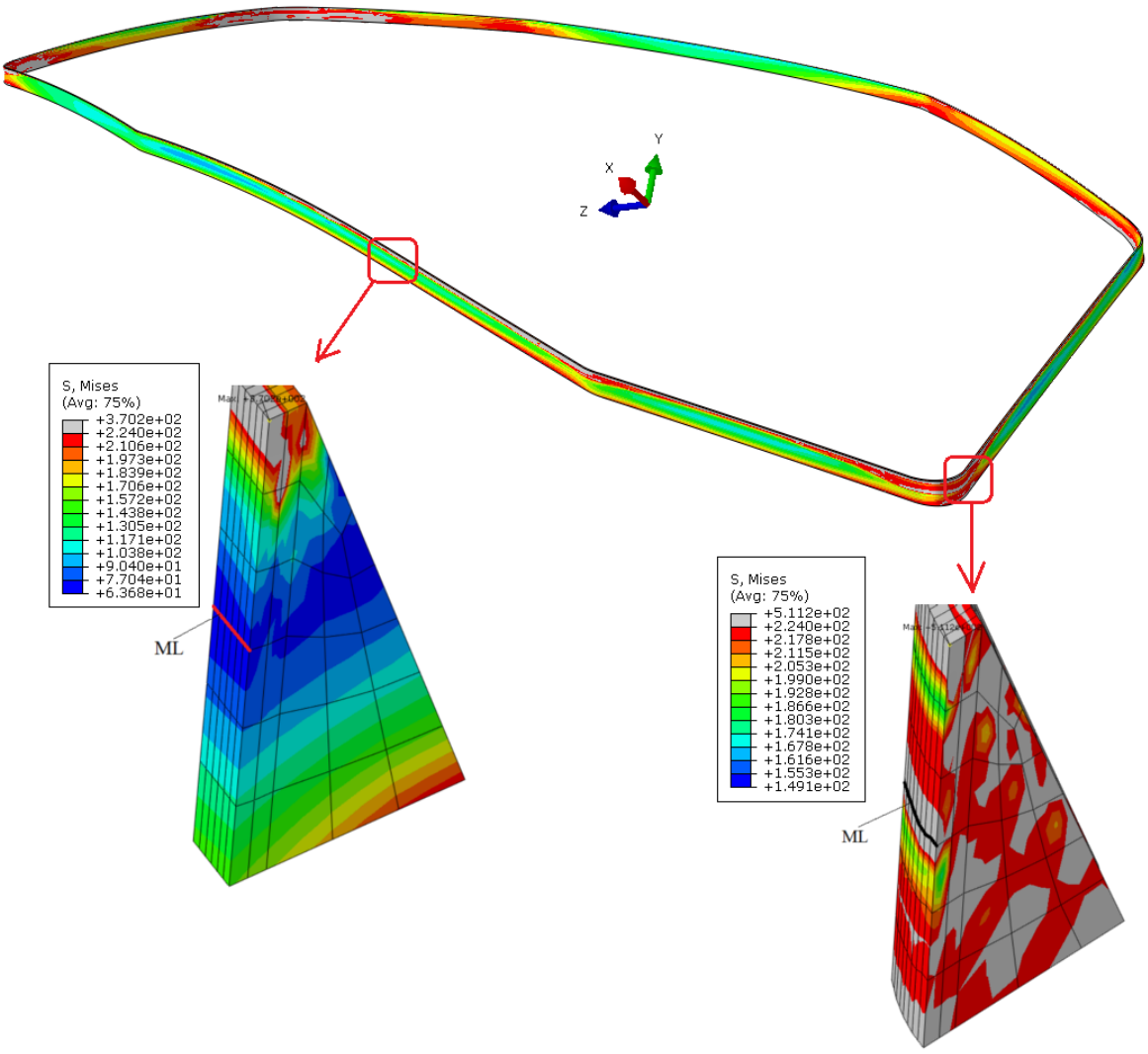


a) b)

Figure 15. Von Mises Stress (MPa) distribution in the cross section of the welding seam: a) in the straight part of the weld, b) at the point with the maximal stress of 511 MPa (at weld corner)

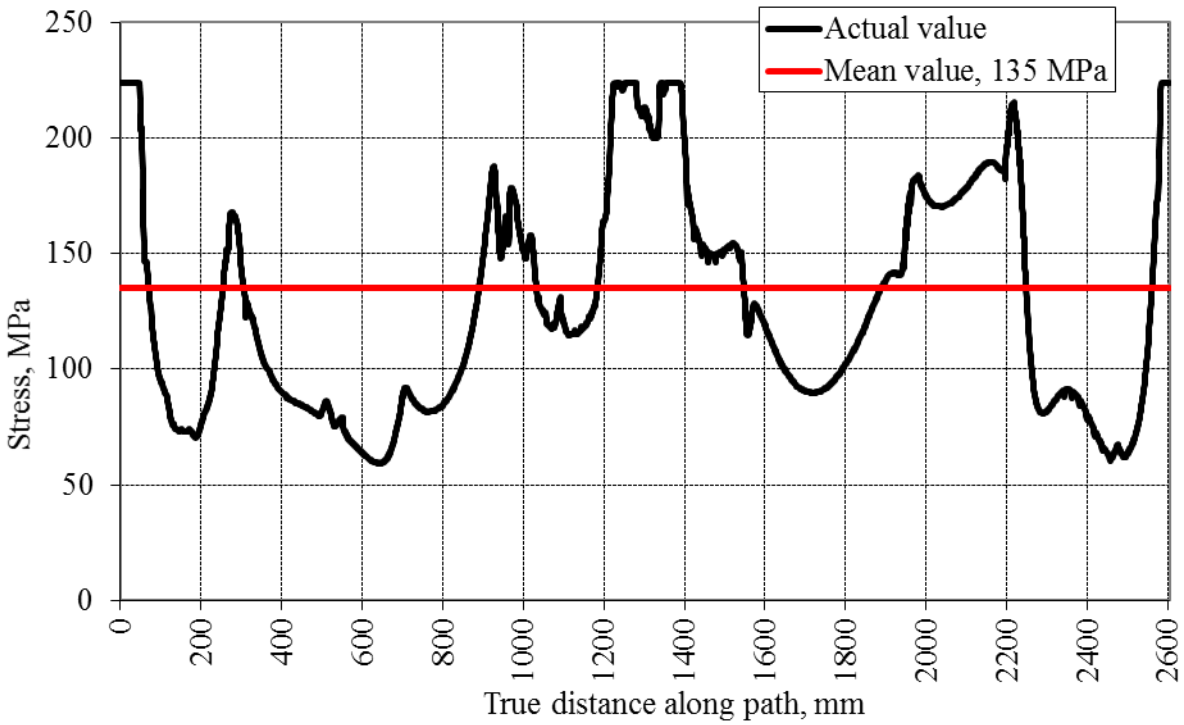


Figure 16. Von Misses stress (MPa) distribution along middle line of weld seam and PV

The distribution of equivalent plastic strain in the cross section of the weld at scale factors 1 (a) and 3 (b) is presented in Figure 17. The plastic strain in the cross section of the weld does not exceed 0.28% at SF=1, and 3.11% at SF = 3. The maximal equivalent plastic strain zones are located on the weld tip and reaches 3.4 % at SF = 1, and 37% at SF = 3.

The additional cyclic loads due to coolant pressure variation, cryostat evacuation procedure, possible PV adjustment, temperature gradients etc. were not evaluated. However the loads during the operation of the W7-X are low cyclic ones and temperature gradient is to be reduced by installation of port liners. The repetitive plastic cycles could have an influence on and therefore decrease the scale factor in which the yielding of the equivalent plastic strain could occur. Also it should be noted that the fragment of the PV which was modelled has been selected based on recommendations from designers, and the influence of the modelled PV area was not evaluated in the structural integrity analysis.

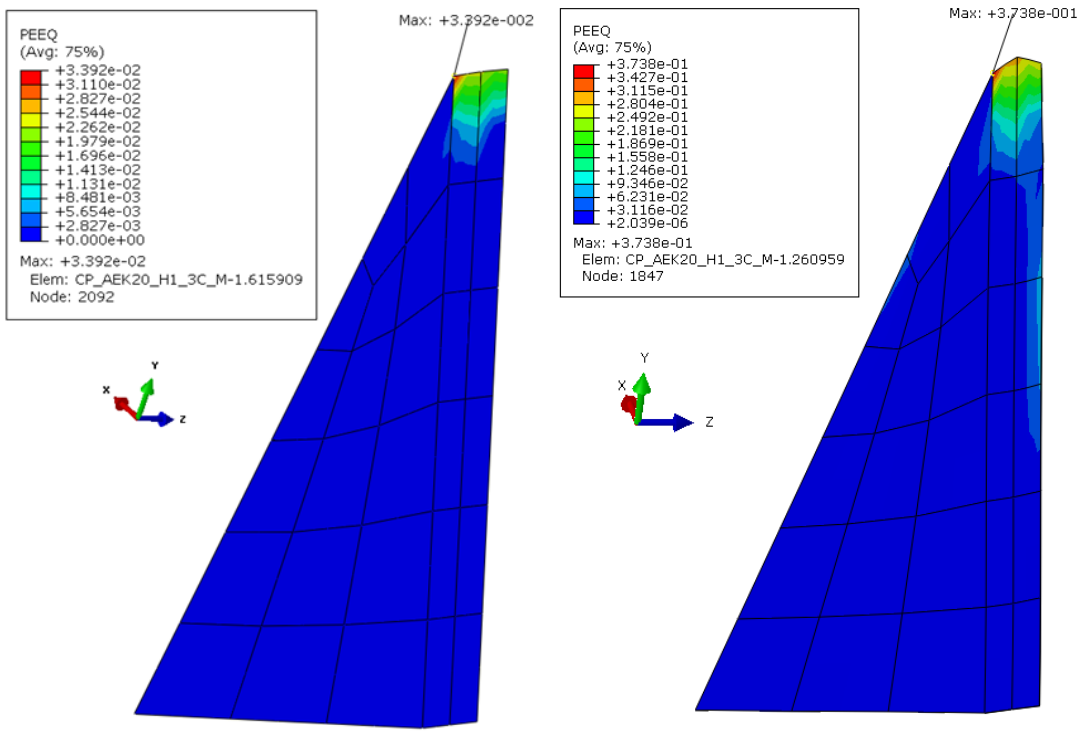


a) b)

Figure 17. Distribution of equivalent plastic strain in the cross section of the central part of the AEK20 port weld with the maximal stress at scale factor 1 (a) and 3 (b)

## 4. Summary of analysis results of the ports

As it is mentioned in section 1, the analysis of the welding connection between the ports AEU30 (Fig. 18-a), AEQ20 (Fig. 18-b), AEK20 and the PV was performed. The summarised results of performed analysis for all ports are presented in this section.

The analysis of the welded connection between the ports AEU30, AEQ20, AEK20 and the PV was performed until the scale factor of 3 was reached. These ports were analysed with a gap of 1 mm. Additionally the analysis of the port AEU30 with a gap of 6 mm was performed. In this paper, results of a detailed limit analysis were presented for the port AEK20 only.

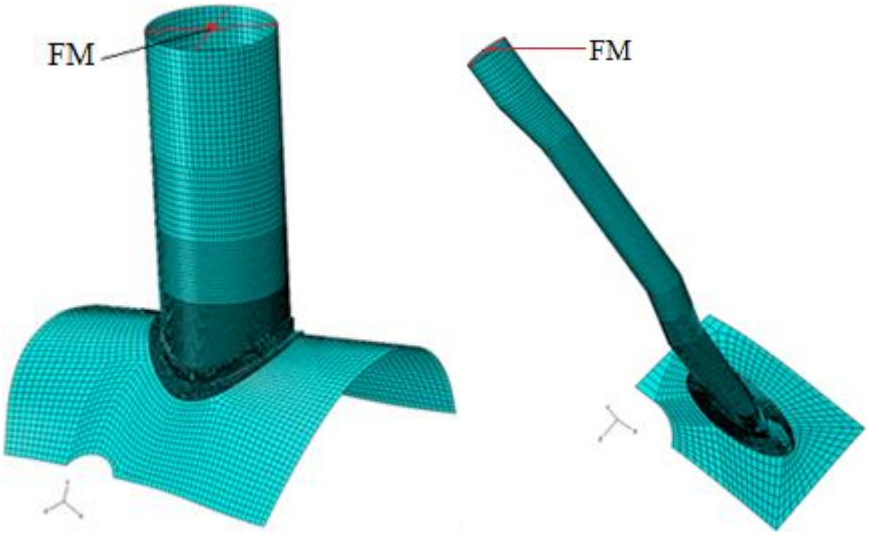


a) b)

Figure 18. FE models of the welded connection between the ports and the PV shell: a) AEU30, b) AEQ20

The summarized magnitude of displacement of the FM point for all models (including the AEK20 port results as well) until the scale factor of 3 is reached and the weld efficiency factor of $K_{weld}$ = 0.7 are presented in Figure 19.

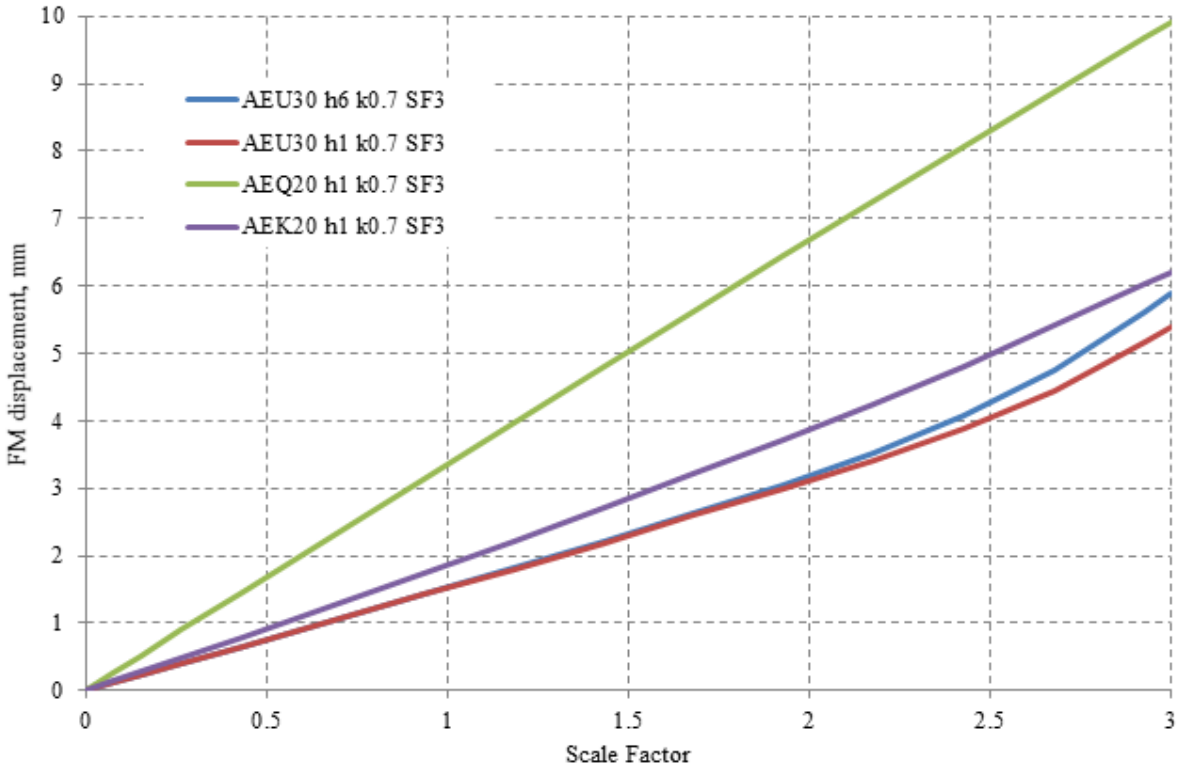


Figure 19. Displacement (mm) of the force-moment application point

The displacements of the port AEU30 with the gaps of 6 mm and 1 mm are presented in Figure 19. The results show that the displacement of the welding seam at the port AEU30 with a gap of 6 mm has reached 5.9 mm. Displacements for both 1 mm and 6 mm gaps have

small deviation from linear dependencies in the port AEU. However, the displacements in the port AEU30 with a gap of 6 mm are higher than for the port AEU30 with a gap of 1 mm. The difference in these displacements at the scale factor of 3 is approx. 8.5 percent. The results of analysis show that yielding of the equivalent plastic strain occurs at the port AEU30 with a gap of 6 mm and the yielding of equivalent plastic strain does not occur in the port with a gap of 1 mm until the scale factor of 3 is reached.

The displacement of the FM points of the port AEQ20 with a gap of 1 mm in the case when the weld efficiency factor is 0.7, at scale factor 3, is 9.7 mm. Displacements are linear until the scale factor of 3 is reached.

The displacements of the port AEK20 are presented for information only. The results for this port are explained in the previous sections.

According to the results of the analysis, the displacement of the point where loads are applied for all the analyzed ports with a gap of 1 mm increases linearly until the load scale factor SF = 3 is reached. Meanwhile the displacement of the AEU30 port with a gap of 6 mm increases linearly until the load scale factor SF = 2.5 is reached.

## 5. Conclusions

The structural integrity analysis of the welded connections of several ports has been performed. A detailed description of the analysis for the welding seam between the port designed for the installation of NBI (AEK20) and the PV shell with a gap of 1 mm is used as a typical example. The geometrical 3D CAD model was developed using the SolidWorks software. The finite element model of the AEK port (640284 elements and 2835090 nodes) was prepared using the ABAQUS computer code. Different increment sizes were applied to the loading steps in the limit analysis. The large increment was used in case of the linear displacement-scale factor dependency, the smaller increments, in the yielding region, and the smallest increment, in the collapse region.

Stress analysis results show that the stresses in some cross sections of the weld reach the yield limit plasticity which is 224 MPa at the load scale factor of 3. However, the mean value of stresses along the middle line of the weld seam and the PV (the perimeter of the weld) is only 135 MPa. The influence of these plastic zones in the weld has a moderate effect on the structural integrity of the whole structure.

According to the results of the limit analysis the displacement of the point where loads are applied increases linearly until the load scale factor of SF = 3.8 is reached. The yielding of displacement occurs from SF = 3.8 to SF = 4.5. After the load scale factor of SF = 4.5 is reached, the displacement starts to increase very rapidly. The convergence of the FE analysis

is lost over SF= 6 for the version of analysis v3, and that means that the stability of the port AEK20 with a gap of 1 mm is lost. Therefore, it can be concluded that the limit load is reached at the load scale factor of 6. In case of the analysed ports AEU30 and AEQ20 the displacement of the point where loads are applied increase linearly for these ports until the load scale factor SF = 2.5 is reached. Therefore, from the results of the analysis it is possible to conclude that the proposed welding between the plasma vessel and the analysed ports fully meets the structural requirements. The main scaling coefficient corresponding to the main critical load is above the minimum acceptable value of 1.5.

It should be noted that it is possible that additional cyclic loads might further influence the results. Besides, a structural integrity analysis of the PV shell in the vicinity of the welded connection was not performed due to a complicated geometry of this component. However, the safety factor that was used in the analysis is high and the number of load cycles is low, therefore there should be no doubts about the structural integrity of the analyzed cryostat welds.

**Acknowledgement**

"This work has been carried out within the framework of the EUROfusion Consortium and has received funding from the Euratom research and training programme 2014-2018 under grant agreement No 633053. The views and opinions expressed herein do not necessarily reflect those of the European Commission."

**References**


[1] J.-H. Feist, J. Knauer, System specification. Wendelstein 7-X – Basic Machine, Report, Nr. 1-NBB, S-5001. Max-Plank-Institut für Plasma Physik, 1999.

[2] H.-S. Bosch, H. van den Brand, R. J. E. Jaspers, P. Urlings et al., Technical challenges in the construction of steady-state stellarator Wendelstein 7-X, Nucl. Fusion, ISSN 0029-5515, Vol. 53, No. 12 (2013) 1-16.

[3] H.-S. Bosch, R. Brakel, V. Bykov et al., Final integration, commissioning and start of the Wendelstein 7-X stellarator operation, proceedings of 26th IAEA Fusion Energy Conference, Kyoto, Japan, 17–22 October 2016.

[4] L. Wegener, Status of Wendelstein 7-X construction, Fusion. Eng. Des. 84 (2009) 106–112.

[5] G. Dundulis, R. Janulionis, R. Karalevicius, The Application of Leak Before Break Concept to W7-X Target Module, Fusion. Eng. Des. 88 (2013) 3007–3013.

[6] Request for Limit Analysis of the Port Welds between the Plasma Vessel and the Ports in the W7-X Cryostat System, Max-Planck-Institut for Plasmphysik, 1-GXA40M-S0001.1.

[7] T. Koppe, A. Cardella, B. Missal, et al., Overview of main-mechanical-components and critical manufacturing aspects of the Wendelstein 7-X cryostat, Fusion. Eng. Des. 86 (2011) 716–719.

[8] V. Bykov, J. Fellinger, F. Schauer, M. Köppen, K. Egorov, P. van Eeten, A. Dudek, T. Andreeva, Specific Features of Wendelstein 7-X Structural Analyses, IEEE Transaction on Plasma Science, Vol. 42, No. 3, March 2014, pp. 690-697.

[9] Plastic Analysis and Design of Steel Structures, Edited by M. Bill Wong, ISBN: 978-0-7506-8298-5, Elsevier Ltd, 2009.

[10] P. Yanga, Y. Liua, Y. Ohtakeb, H. Yuana, Z. Cen, Limit analysis based on a modified elastic compensation method for nozzle-to-cylinder junctions, Int. J. Pres. Ves. Pip.82 (2005) 770–776.

[11] B. Milošević, M. Mijalković, Ž. Petrović, M. Hadžimujović, The Application of the Limit Analysis Theorem and the Adaptation Theorem for Determining the Failure Load of Continuous Beams, Scientific Technical Review, Vol. 60, No. 3-4 (2010) 82-92.

[12] W. H. Yang, Large deformation of structures by sequential limit analysis, Int. J. Solids. Structures. Vol. 30. No. 7, (1993) 1001-1013,.

[13] J. Wust, W. Wagner, Systematic Prediction of Yield-Line Configurations for Arbitrary Polygonal Plates, Universit at Karlsruhe, Mitteilung 2 (2007).

[14] K. Krabbenhoft, L. Damkilde, Lower bound limit analysis of slabs with nonlinear yield criteria, Comput. Struct. 80 (2002) 2043–2057.

[15] F. Z. Xuan, P. N. Li, Finite element-based limit load of piping branch junctions under combined loadings, Nucl. Eng. Des. 231 (2004) 141–150.

[16] Y. J. Kima, K. H. Leea, C. Y. Parkb, Limit loads for thin-walled piping branch junctions under internal pressure and in-plane bending, Int. J. Pres. Ves. Pip.83 (2006) 645–653.

[17] D. Plancq, M.N. Berton, Limit analysis based on elastic compensation method of branch pipe tee connection under internal pressure and out-of-plane moment loading, Int. J. Pres. Ves. Pip.75 (1998) 819–825.

[18] K. P. Kim, H. Huh, Dynamic limit analysis formulation for impact simulationof structural members, Int. J. Solids Struct. 43 (2006) 6488–6501.

[19] V. Bykov, F. Schauer, K. Egorov, et al., Structural analysis of W7-X: From design to assembly and operation, Fusion. Eng. Des. 86 (2011) 645–650.

[20] Ł. Ciupinski, G. Krzesinski, P. Marek, et al., Limit analysis of W7-X critical magnet system components with consideration of material serration effect, Fusion. Eng. Des. 86 (2011) 1501-1505.

[21] E. Briani, C. Gianini, F. Lucca, A. Marin, J. Fellinger, V. Bykov, Limit analysis of narrow support elements in W7-X considering the serration effect of the stress-strain relation at 4K, Fusion. Eng. Des. 86 (2011) 1462-1465.

[22] V. Bykov, F. Schauer, K. Egorov, et al., Structural analysis of W7-X: Overview, Fusion. Eng. Des. 84 (2009) 215–219.

[23] http://www.solidworks.com, 2015.

[24] Abaqus/Standard, 2011. User's Manual Volume IV, Version 6.10.